On the Time Decay constant of AEM systems: A Semi- Heuristic Algorithm to validate calculations.

José Manuel Martínez
2-572 Ampere Ave.
Laval, Canada, H7N5W9
Phone: 438-22-3366
E-mail: jmartinez2050@gmail.com

Richard Smith
Harquail School of Earth Sciences
Laurentian University
935 Ramsey Lake Road, Sudbury, ON, Canada, P3E 2C6, RSSmith@laurentian.ca
Danilo Diaz Vazquez
Departamento de Ciencias Fisicas, Universidad Andres Bello, Autopista Concepcion-Talcahuano 7100, Talcahuano, Chile
Email: danilodiaz@unab.cl

PREPRINT VERSION:
Subsequently published as

Martínez, José Manuel, Richard Smith & Danilo Díaz Vázquez, 2020, On the time decay constant of AEM systems: a semi-heuristic algorithm to validate calculations: Exploration Geophysics, 51, 94-107, DOI: 10.1080/08123985.2019.1662291
https://www.tandfonline.com/eprint/S9MZPPKJIRW3FYWNWFDV/full?target=10.1080/08123985.2019.1662291

ABSTRACT

The time decay constant or "tau" of airborne EM systems (AEM) is commonly used to indicate the presence and the relative conductivity or conductance of conductors in the survey area. In fact, it is not a constant since it depends on: the system; the survey design and the method of calculation. The system dependence is a consequence of parameters relating to the acquisition and *pre*– and *post*– processing of the signal. Here we propose a method for calculating tau, which is simply the time at which the transient voltage decays to 37%, or V_{37}, of some initial value. The model utilises a semi-heuristic algorithm that estimates V_{37} for each transient in the database and then it calculates the delay time that voltage is measures, which is the estimates tau value. No calculation is involved with the data, instead tau is given by a weighted average of the delay times associated with the windows either side of the V_{37} value. We illustrate how this algorithm works using data collected by MEGATEM II in the Reid-Mahaffy test site. Results shown a good agreement between tau-grids reported in previous studies and those calculated with our V_{37} – method. To account for all effects coming from the acquisition and processing of EM data, the algorithm allows the emphasis to be shifted from early to late time parts of the transient. It is envisage that since this method does not apply any mathematical operation to the data it may serve as a robust means of for validating other methods.

Key Words: time decay constant, tau, semi-heuristic method, large EM database, fast calculation, time domain.

INTRODUCTION

A map of tau with electromagnetics (EM) anomalies superimposed is a common derivable of AEM surveys, as it summarizes the EM signature of the area. One of the first heuristic methods for calculation of tau was reported by Nelson and Morris (1969) where the tau was calculated using the ratio between two late off-time windows. In this case, the interpreter needs to judge by experience which late time windows are suitable for calculations. Despite of problems, the methodology could be used to summarize an entire survey. Grant and West (1965) devised a method to determine the tau for frequency-domain data by taking the ratio between the in-phase and quadrature responses. More insight into the nature of transient decays was provided by Palacky and West (1973), who showed that these decay transients are described at early times ($t < tau$) by a power law while for late times ($t > tau$) by multiple exponential decays. This approach has since been extensively applied to understand and explain both synthetic and field EM data. Furthers studies carried out by Kaufman (1965, 1978) demonstrated that for late times (t>tau) a single exponential function was appropriate to describe the presence of deep seated conductive bodies. Consequently, the single exponential and power-law behaviour of the decay gained popularity and it was further studied by Bartel and Hohmann (1985) and Bartel and Becker (1988), and others. These studies undertook forward modelling to establish very useful empirical formulas for calculating tau based on: the terrain clearance, depth, size and conductivity contrast. Other methods like singular value decomposition into multiple exponentials by Stolz and Macnae, (1998) and the matrix pencil method by Chen and Macnae (1998) are good trade-off between time of computation and the reproducability of τ. Currently, it is widely accepted that late transients are well described by a single exponential decay. Commonly, tau grids are calculated by fitting a single exponential decay curve to the EM data, e.g. Smith and Lee, (2001).

The aim of this study was to find a method to determine tau with as few operations to the data as possible. To that end we investigate how EM data is acquired from current AEM systems and found out that there are several engineering trade-offs made during the making of an AEM system that impact on the decay transients and thus tau. Upon analysing these effects our semi-heuristic method to calculate tau for large EM datasets emerged. The method is based on the late-time transients being described by a single exponential function. In that case tau is simply the time at which the voltage measured by receivers decay to 37% of its initial value. Therefore, an algorithm seeks this value, denoted V_{37} , for each transient in the database. The tau value is a weighted average of the delay times of the two windows between which the value of V_{37} occurs (described in more detail below). There is not mathematical operation involving the EM measurements, so measurement noise does not have a large impact on the estimated tau value. The worse impact usually no worse than moving the tau estimate one time window earlier or later.

The rationale behind tau measurements

Why is tau EM system dependent?

The tau is system dependent because of both the transmission and reception of primary and secondary fields are system dependent. To illustrate this strong dependence, let's consider the two conditions for which tau is system independent. They are: 1) a perfect square pulse (i.e. rise and fall times occur instantaneously) with at least a 50% duty cycle and 2) voltages measured by receivers that are only measuring the voltages in the off-time when there is no primary field. If these two ideal conditions are met, then the decay transients are those illustrated in Figure 1B.

{INSERT FIGURE 1 HERE}

In the idealized waveform of Figure 1,where the current rises from zero to I_{peak} instantaneously and the falls instantaneously at the end of the pulse. There is a transient response from the target for every time a current switch occurs. Note that in the entire full-cycle, *T* there is four responses (i.e. one occurring after each switching). These responses are not hypothetical they are present in all AEM systems but they are not always recorded, for reasons discussed later. In our illustrative example on Figure 1B, the same target is excited, so there is no differences in these decay transients, i.e., $\tau_1 = \tau_2 = \tau_3 = \tau_4$. When recording over a whole duty cycle, *T*, the tau can be determined by stacking these four responses and apply any of the previous methods described in the introduction. Or alternatively, one can estimate the maximum voltage response from the target, i.e. V_0 and use this to calculate the V_{37}, which is 37% of this initial value and determine the time that this occurs, a process which will be described in more detail later on. Note that only and only if there is perfect reception where the voltage measured by the receiver are solely due to the responses from targets, will both the decay transients and thus tau be system independent. In practice it is not possible to switch the current on or off instantaneously. Hence, the secondary will not be the only field present in the measurements, there will also be a primary field. The reason for the non-ideal nature of waveforms is that the current has to pass through cables, and they have inductances, which introduce a delay to the switching process. This means that there is a changing primary field, which will induce a voltage in the receiver coil. This primary field can six orders of magnitude larger than the voltages from the response of targets. This is attempted to be addressed by introducing an attenuation and/or bucking mechanism so as to literally avoid burning the conditioning electronics of the receiver. Each electronic engineer designing EM systems has their own approaches of acquiring EM data to avoid these problems and specific approaches to pre and post processing data. These approaches can make tau system dependent. Hence one may wonder what percentage of a tau estimate reflects the target and not the sustem. In our view,

the more clarity we gain about how all these factors interplaying, the better tau can be associated with the target and exclude the system and/or method of calculation.

In practice, the waveform of an AEM system is driven by some form of square pulse as depicted in Figure 2.

Effect of synchronous acquisition

The cornerstone of acquisition of existing AEM systems relies on synchronous acquisition schemes which utilises gates (Macnae et al., 1984), such as those in Figure 2 labelled W1, W2, W3, and so on. Throughout these windows the analog signal picked by the receiver sensors can be converted into digital form (details are given in the next section). One can imagine when these gates are open during the off-time, the data acquisition system (DAS) collects samples, N_s (see open circle in Figure 2B) depending on the system sampling rate, *SR* (more details of which are given later on). For instance, if the DAS has an analog module rated at *SR* =250 kHz, the very first sample gathered by the system will come after 4μs (this calculation is performed below) after the primary field has been shut down. These windows are designed such that the number of samples in each window increases exponentially for later windows Wi. It is expected that open circles in each window are averaged in some wayi.e., $\sum_{i=1}^{N} V_i/_N$. The simple average works well if the window is narrow and the response decays approximately linearly in the window. However, for late time (*t*>*tau*) some other statistical estimator, like the median may offer a better statistical descriptor (p.656 Press et al., 2007). However, there might be other undocumented processes used to improve the results like using more samples from outside the windows, or arbitrarily removing a late-time asymptote or a non-decaying component (as is done in the TEMPEST system; Lane et al., 2000). Obviously, the procedures used to process the raw data will determine the decay transients and thus tau.

{INSERT FIGURE 2 HERE}

Effect of receiver coils

Transients at the receiver (Rx) falloff rapidly lasting just a few milliseconds before they sink into noise. Electrically Rx are designed to have low noise figures (in the order of pT) and flat responses with a bandwidth of about 20kHz (Macnae, 2012). The most desirable electrical characteristics of an Rx is to have low impedance (in order to have low noise figures) and the highest inductance possible (to be able to pick small varying secondary magnetic fields). These two physical properties are contradictory, leading to a trade-off between inductance and impedance for an inductive receiver at low frequency ranges (Martinez et al., 2014). High inductance means smaller wire gauges and lots of turns and that increase the impedance of the coil drastically. One solution to attain high inductances in the Rx, with fewer turns, is to utilising permeable core materials to amplify the magnetic field. The only inconvenience is that these materials impart non-linearity to the pre-amplification stages (Neri, 1996). A close-loop compensation network is necessary to flatten the electromagnetic field responses within the bandwidth. Another solution, since the peak voltage from targets, i.e., V_o depends on r_{RX}^2, would be to increase the Rx radius, r_{RX}. However, since the voltage induced by the primary field, V_p is up to six orders of magnitude larger than V_o this radius is restricted to r_{RX}~0.6m. Note that, V_o is determined by the physical dimension of the Rx and it is nothing but $2\pi\mu_0 A_{eff}$, where μ_0 and A_{eff} are the permeability of the free space and the effective area, $A_{eff} = \pi r_{RX}^2 N_{Rx}$ of the Rx, respectively. Because of these differences between V_p and V_o a dual preamplifier is needed in an AEM systems. The amplifier for the secondary field attenuates during T_{ON} while amplifies during T_{OFF}. This strong attenuation impedes recording of the on-time response from the target

atone limitation of the receiver is that there is a lower limit of voltage resolution, V_R for each AEM system. This is, the minimum voltage that can be converted from analog to digital. In other words, V_R depends on the ADC bit resolution of the DAS. For instance, if the DAS has

an analog module capable of measuring voltages between 0 and 5V and the ADC encodes its data using 16 bits, this will give: V_R =5V/2^{16}=76.3μV. In other words the lowest voltage the EM system can detect is just 76.3μV and the maximum is less than 5V. Hence several pre-amplification stages are required. Knowing the total gain, G of the EM system would be sufficient to obtain transients reported in the EM database from the raw data. In some cases the measurments are normalized, with respect to primary magnetic fields recordings, e.g. $\mathrm{B(ppm)} = \mathrm{V_o G/V_p} \times 10^6$ in [nT/V]. Sometimes $\mathrm{V_p}$ may be expressed in ADC units ($\mathrm{V_p(ADC)} = 2 \times 10^4 \mathrm{ADC}$), that one can convert to voltage using V_R. That is: $\mathrm{V_p(V)}$ = $2 \times 10^4 \mathrm{ADC} \times 76.3\mu\mathrm{V/ADC}$ = 1.5V.

The above briefly describes the choices made for how an AEM system acquires data, and these can impact how decay transients are recorded.

Effect of data encodings

One way to improve the SNR is by acquiring more samples N_s per windows sampled (Eaton, 2013) by increasing the system's sampling rate, *SR*. For instance, if the DAS of the EM system is rated at 40 MHz with one tick every 25ns; having an analog module rated at *SR* = 250 kHz; its first sample will come after 4μs $\left(= \frac{40\cancel{\mathrm{M}}\mathrm{Hz}}{0.25\cancel{\mathrm{M}}\mathrm{Hz}} \times 0.025\mu\mathrm{s}\right)$. The latter is some time referred to as the as point value. Nowadays, the *SR* of commercial and non-commercial system is set around SR = 250 kHz (Allard, 2007). Ramping up the *SR* up is not a straight-forward task as the volume of data to be streamed is in the order of megabit/s and special chopping and streaming algorithms are needed right on the memory of the microcontrollers to cope with such a huge volume of data (Eaton, 2013). To have an idea of the order of streaming happening in an AEM system, if the system has a SR=500 kHz and the waveform repeats at a base frequency, f_b = 30 Hz; then $N_s = \frac{SR}{2f_b} = \frac{500\mathrm{kHz}}{60}$ = 8333.3 samples per $T_{\mathrm{T}/2}$. Let's say these samples are encoded using 32 bits, then the number of bits in $T_{\mathrm{T}/2}$ is 266665.6 (8333.3x32) bits. As there

200 are 60 half cycles per second, then in 1s there are 1,599,993.6 (266665.6x60) bits (or 2Mb/s)
201 and if the system has three Rx then it will be 6MB/s. That may not sound much data in today's
202 line communication systems, however the catch for an AEM system is that the DAS handles
203 several mixed signals (analog & digital signals) requiring algorithms to ensure precise
204 triggering, synchronization , streaming and control. And all of them have to reside on the
205 memory of the microcontroller to handle all system request. Therefore control, communication
206 and steaming protocols needs to be optimized in order to avoid overflow, lags so as to ensure
207 than data is not lost.
208 All the above bring some clarity on the way the AEM system acquire convert and encode its
209 data to form the decay transients. Manufacturer are quite familiar with these issues but not all
210 interpreter are. However, it is important to know these issues in order to understand how tau
211 depends on a particular AEM system and how to compare the tau gathered from two different
212 AEM systems.
213 Effect of the transmitter moment + switching
214 Significant engineering efforts are required to increase the moment (power) of an AEM, where
215 the moment, $m = NIA$. This is as important because: 1) theoretically the measured signal
216 depends linearly with m and 2) in practice by doubling the duty cycle of the current wave form
217 will guarantee higher target responses (Becker et al., 1984). Often there is a tendency to use
218 the peak current, I_{peak}, without including the duty cycle, in order to calculate m (see for
219 instance I_{peak} and I in Figure 2B). The reason of this widespread confusion comes from the
220 fact that in frequency domain systems the current is always ON, i.e. 100% duty cycle. For AEM
221 system this is not the case. For instance, for the MegaTEM system, I_{peak}=710 A and when the
222 system is tuned to fire at 30 Hz and 90 Hz base frequencies, their corresponding duty cycle are
223 24% and 41%, respectively. Details regarding this calculation is provided in the result section.

This means the current for these frequencies are I = 710 x 0.24 A=170 A at 30 Hz. This value to be entered in the calculation of m and not I=710 A.

The tau value can change depending on the shape of the waveform, which elicits responses from targets by creating a sharp rise or fall of the pulse of current (see the ideal situation in Figure 1A). The current is induced in a target according to Faraday's law, which states the electric field induced by the primary is directly proportional to the rate of change of the primary pulse, i.e. $\Delta I_p/\Delta t$ (see for instance, slow and fast switching in Figure 2A). The sharper $\Delta I_p/\Delta t$, the more high frequency harmonics are imparted into the target. To obtain sharper rises or falls (via shorter ramps) is one technical aspect that is difficult to achieve in an AEM system. This is as such because: 1) the switching mechanism behind generation of primary magnetic fields need to be fully digital and controlled at frequencies of at least 500 kHz (Saini et al., 2014), and 2) the total inductance of the transmitter , Tx, (including transmitter cables) are rarely optimized.

At this point one may wonder why a fast switching is of importance for tau? The answer is given by comparing decay transients from slow and fast switching (see black and red decay transients in Figure 2B). A fast current cut-off comes with shorter t_{RAMP}, (i.e., the time the EM system takes to bring the current up or down to zero). One way to achieve a t_{RAMP} of a few microseconds is by imparting few Amperes into the Tx. That is the idea behind the dual moment deployed by the Skytem system described by Sørensen and Auken (2004). Obviously if t_{RAMP} takes too long, then high-frequency or near-surface information is reduced. For instance, in the illustrative example of Figure 2B, the first four off-time windows (W9-W11) available for a fast switching system (black decay curve) are smaller amplitude when they eventually occur in W12-W14 in the case of the slow switching transmission system (red decay transient).

248

Effect of bucking/shielding mechanisms

Another difficulty with EM systems is that the voltage of transmission, V_p can be six orders of magnitude greater than the secondary. The variety of solutions to this issue results in a wide variety of EM systems configurations. One solution is to use a dual preamplifier. One amplifier will attenuate the signal during T_{ON} when the primary is large and the second will amplify it during T_{OFF} when the small primary is present. Another solution used by the VTEM systems is to cancel the primary fields in a receiver by injecting the same pulse of current but with reverse polarity into a more proximal transmitter bucking coil (Kuzmin and Morison, 2013). The disadvantage of this solution is that m will be slightly lower, compared to the situation where there is no bucking coil, due to the field of the bucking coil, opposing that of the main transmitter therefore lowering the overall system moment (Xiao et al. 2017). Yet another solution is to null couple the primary field with the receiver, for example above the transmitter wire where the field is horizontal and a receiver loop is horizontal. Of course, the problem can also be avoided by placing the receiver a larger distance from the transmitter for example ~40 m above and 20 m off centre.

Tau & the survey design

Adjusting the survey design is another way to improve the signal-to-noise ratio (SNR) of the AEM system.

For example say T_s is the survey sampling time, which is the time elapsed between two set of lateral (i.e. along the flight direction) measurements. And the distance between these measurement is d. The former sometimes is referred as the lateral resolution of the survey. Then, the sampling frequency of this survey is: $f_s = \frac{v_{heli}}{d}$; where v_{heli} is the speed of the helicopter. The number of transients within each survey sample is $N_t = \frac{2f_b}{f_s}$. Suppose an AEM survey is conducted at a base frequency $f_b = 30$ Hz; and the transients are stacked over a

sample interval of T_s =1 s, so f_s=1/T_s=1 Hz). Then, if v_{heli} is on average 40 knots or 21m/s, then will result in d of ~21 m and there will be $N_t = \frac{2\times30}{1}$ = 60 transients available for stacking for every 21m flown. If we double v_{heli} to 42 m/s while keeping T_s=1 s; N_t will remain unchanged and from the spatial resolution will deteriorate as d increases to 42 m and noise due to vibration at higher speeds sink the signal into the noise way sooner. One way to improve the survey while keeping v_{heli} fixed e.g., at 21 m/s is using T_s = 4 s). In that case, f_s = 0.25 Hz resulting in $N_t = 240$ transients for every 42 m flown.

Effect of filtering and stacking

While in flight an AEM system is subject to motion, vibrations and bird swings (Davis, 2008). Typically, AEM systems have an analog low-pass anti-alias filter for each receiver at the input of the preamplifier to remove high-frequency components. In addition most of them remove the 50Hz/60Hz power-line signal by digitally stacking the data at a frequency that has the power-line signal as an even harmonic. Once the signal is in a digital mode the most common workflow of processing is removing unwanted spherics and then apply a series of non-linear and linear filters to the EM database. Details about the type of filters and their characteristics are rarely disclosed and without doubt they impact the transients and thus tau. This workflow can deteriorate the main peak of anomalies. Typically, longer duration filters reduce the high-frequency noise floor noise but at the expense of decreasing the main anomaly peaks. There is an alternative workflow and deals with our illustrative example of Figure 2B. It is rather convenient to estimate the transient by its corresponding windows by proposing a statistic descriptor for each window to bring the open circle (see Figure 2B) to full dots before the first stacking occurs. In that way one can reduce, if not entirely avoided all filtering the EM data is subject to. If each transient is process in that manner in every half-cycle; the next will be removing its trends (see straight line draw in Figure 2B) to make stacking possible. As for stacking concerned, one can use the mean value or median depending on the noise level of the

system. To the best of our knowledge this workflow strategy based on the actual acquisition of the EM signal never has been used in the processing of the data acquired by AEM system. Indeed, it is more appealing as these window filters remove the high frequency noise, but use the shortest length possible.

V_{37} – METHOD

Since the late time response is described by a single exponential function (Kaufman, 1978), the late time voltage response for the step and impulse excitations are respectively:

{INSERT EQUATION 1, HERE}

One way to determine tau is by estimating the time at which the step response signal has decayed to 37% of its initial value, V_0. That is if t_j is the window centre time of the jth window (see Figure 2B), i.e. $t_j = \frac{t_{j-1}+t_{j+1}}{2}$, then if $t_j = \tau$ for the step response yields: $V(t_j = \tau) = V_{37} = \frac{V_0}{e} = 0.3679V_0$. Figure 3 illustrates the scheme used in this paper for computation of τ. Note that on the x-axis symbols t_{j-1} and t_j represent the two consecutive centred time windows where the amplitudes of the decay at these times are above and below, V_{37}, i.e. $V_{j-1} > V_{37} > V_j$. Rarely does τ corresponds with a centre time that is given in the time window table. One may think to calculate τ simply by taking the average time from which V_{37} falls into, i.e. $t_m = (t_{j-1} + t_j)/2$, however for the situation depicted in Figure 3 that would be an overestimate. The other option is to use a simple weighted-average interpolation. That is:

{INSERT EQUATION 2, HERE}

Weights ω_j and ω_{j-1} are values between 0 to 1 and they give a measurement of proximity of V_{j-1} and V_j with regards to V_{37}. For instance, in the example of Figure 3, V_{37} falls closer to the measurement V_{j-1} than V_j. That is:

{INSERT EQUATION 3, HERE}

{INSERT EQUATION 4, HERE}

Maximum weights are equal to 1 and this is when V_{j-1}=V_{37} or V_j =V_{37}. In the case τ is given by the central time gate and not calculated by equation (3). Otherwise these weights are less than one and the higher they are the closer τ will be from either t_{j-1} or t_j (see Figure 3).

{INSERT FIGURE 3, HERE}

Exponential functions decay monotonically, so it is not physical possible that the decay voltage at time "$t+1$" be greater than at time "t". Therefore the first thing the V_{37} – method does is to excluded any transients that do not monotonically decay.

RESULTS

The Reid-Mahaffy site is a test site in Canada is an area covered by glacial overburden and underlain by Archean (~2.7 b.y.) mafic to intermediate metavolcanic rocks in the south, and felsic to intermediate metavolcanic rocks in the north, with roughly an east-west-striking stratigraphy (Ayer and Trowell, 1998).

The V_{37}-method was tested on two available EM datasets provided by the Ontario Geological Survey (OGS 2003, 2004) collected over this site. The region was surveyed twice by the MEGATEM II time-domain electromagnetic system. The 2003 data set were collected with a base frequency f_b= 90 Hz, while the 2004 data set used f_b=30 Hz. In both cases, the survey area was covered using sixteen N-S oriented traverse lines; with a survey line spacing of 200 m. The aircraft was flown at a nominal transmitter altitude of 120 m and a nominal receiver altitude of 70 m. For this system the first five windows corresponds to on-time data, then there are two windows in the off ramp (6 and 7) and finally 13 off-time windows. The sample rate (SR) of the system was 43.4 μs at 90 Hz and 16.3 μs at 30 Hz. The duty cycle was not reported,

however it can be calculated using f_b, the on/off-time and the delay reported, see for instance p.8 on. OGS (2003) for the 90 Hz case. The off and on times are 3175 µs and 2280 µs, respectively and the anti-alias filter delay was 100 µs and this amount should be added to the off-time Hence the half-cycle is 2280+100+3175 =5555 µs , and therefore the duty cycle is 41% [2280/5555]. The peak current was reported as 710 A, therefore the nominal current is *I* = 291 A (710 x 0.41 A). The transmitter has 5 turns and the area of receiver coils was 406 m^2. Therefore, the duty-cycle corrected moment for this survey was m=591 600 (120 x 5 x 406) Am^2. Similar calculation can be performed for f_b=30 Hz, where the on time is typically 4000 µs and the half-cycle 16666 µs yielding a duty cycle of 24%; with the dipole moment 927 000 Am^2, the duty-cycle corrected dipole moment is m =222 000Am^2. Other parameters of the survey can be calculated using the formulations provided in earlier sections and their value are depicted in the Table below.

{INSERT TABLE, HERE}

In the report (OGS, 2004), the EM database "darm1" (at 30 Hz) had several windows for tau calculated. These tau reported were calculated from W8 to W20, which corresponds to 369 µs to 3038 µs after turn-off of the primary field. The standard method used is to fit an exponential $y_{data}=y_0e^{(-t/tau)}$ to the EM decay [see p. 13 OGS (2003)].

The comparison shown thereafter deal with the tau reported in the OGS (2003 and 2004) database window and the one calculated using equation (2). To start the comparisons, the channels of the vertical component magnetic-field Bz (em_bz_final_off) was selected. In the study the earliest channel parsed to the V_{37}-code was window 8. The tau derived was gridded using minimum curvature, which available in many EM database processing software packages.

{INSERT FIGURE 4 HERE}

The only user adjustable parameter is a tolerance to control the number of readings greater than the previous reading. On figure 5, the tolerance was set to 0%, so any transient what showed an increase in any window compared with the previous window was excluded from the tau calculation and the tau value is set to zero.

{INSERT FIGURE 5, HERE}

Clearly, the data from the region just to the north east of the centre has zero tau and an inspection of the database shows that for this area the values of window W20 are higher than W19. By adjusting the tolerance to 15% none of the transients were penalized.

Another feature of the algorithm is that the interpreter can choose which window to assign the value of V_0 before the calculation of tau. To illustrate the impact of different initial windows, we selected the Bz_channel from EM database "darm2", which is the 90 Hz) database from OGS (2004) and calculated tau using window 8 and then window 9 as the initial window Figure 6 and Figure 7 are the grid of the tau calculated using equation (2). In this dataset, the tolerance permitted was set at 5%. Note that the only effect of this tolerance is to include more transients into the calculation of tau and it does not alter the estimate in any form.

{INSERT FIGURE 6 HERE}

{INSERT FIGURE 7 HERE}

Next we apply the method to the dB/dt data set.

Figure 8 illustrates the tau grid of the channel of "em_z_final_off" reported in the darm2 database, OGS(2004) while Figure 9 the one calculated with a tolerance of 5% using the equation (2).

Looking at tau grids calculated (see Figures 5,6,7 and 9) we observe that there are numerous central lows with peaks to the north and south. This is a consequence of the anomaly over a vertical conductor having a peak-trough-peak character on the *z* component (Smith and

391 Keating, 1996). Hence we also tried the new method on the *x* component, which has a large
392 positive peak directly over a vertical conductor (Smith and Keating, 1996).
393 Figure 10 shows the standard tau grid of the channel "em_x_final_off" delivered in the darm2
394 database (OGS 2004) while Figure 11 is the tau grid calculated using (2) with an overall
395 tolerance of 5%. Figure 11 shows less along-line asymmetry artefacts and more features
396 running along the geological strike WNW.
397
398 {INSERT FIGURE 10 HERE}
399
400 {INSERT FIGURE 11 HERE}
401

DISCUSSION

The tau grids calculated using the standard exponential fitting (e.g. Figure 4) and those calculated by the V_{37}-method (see Figure 6) are in agreement. Both show maximum at the same position. There are slight differences in the value of the time constant, possibly as a consequence of the standard method fitting noisy data at late time or the fitting emphasizing the large (early-time) amplitudes.

Being able to select the first window to start and the tolerance applied to transients provides interpreters with a flexible way of calculatingtau so as to enhance features of interest. The entire calculation takes fractions of seconds for a large EM dataset, therefore different scenarios can be tested quickly. For instance, Figure 6 illustrates the tau calculated using the start window 8 (W8) while Figure 7 uses W9. For example, Figure 7 does a better job highlighting anomalies appearing on the north-east side of the map which could be deeper. Same applies to these anomalies found in the central-east side since they EM signatures even when the window to start was W9.

In processing the above, we found that different tolerances were required for darm1 (15%) compared to darm2 (5%). This is because the data in darm1 was acquired with MegaTEM operating at a base frequency of 30 Hz compared to 90 Hz for darm2. The higher base frequency means the number of transients in each stack is tripled and the corrected system moment is nearly three times higher, resulting in more optimal performance at 90 Hz compared with 30 Hz. Furthermore, the duty cycle at 30 Hz is 24 % while at 90 Hz it is 41 %. The more optimal values for 90 Hz explains why the penalty for the darm2 database was only 5% while for darm1 it was 15%. In other words, the information provided in the previous sections is useful as it allows interpreters to assess the weaknesses of a system and to assess the quality of the data generated by a system.

When equation (2) was applied to calculate tau from the impulse response data (e.g. Figure 9) we found with the results were similar to those evident on the tau grid resulting from the standard method (see Figure 8). This may be because the data was gathered with dB/dt sensors and then mathematically converted into the step responses (Smith and Annan, 2000).

A comparison of Figures 10 and 11, shows a number of interesting features. Firstly, there are less north-south asymmetry effects (highs on alternate line directions) that are evident in Figure 11 and secondly, the geological features running east-west and west of north west are narrower. This could be a consequence of an emphasis on slightly different decay times in the figures. Adjusting the window for the initial time might change the look of the image somewhat, but the methods consider a different range of times and use different method so identical results are not expected. If late-time information is required, then the window for V_0 can be made later.

CONCLUSIONS

The practical implementation of AEM system makes tau system and processing dependent.. The V_{37} method proposed here is simpler and less dependent on the system and the data processing . The method has some flexibility in that the initial time can be moved, to place emphasis on earlier or later parts of the decay. The resulting tau grids can be used to identify areas that can be used for more sophisticated processing or inversion methods.

ACKNOWLEDGEMENTS

We would like to thanks Geo Data Solutions GDS Inc. for incentives and motivations to investigate in this subject. We would like to thanks Pierre Keating and Dr. Combrinck for their valuable suggestions. This work has been supported in part by the IRAP grant #849675.

450

REFERENCES

Allard M., 2007, On the Origin of the HTEM Species, in B. Milkereit, ed., Proceeding of Exploration 07: Fifth Decennial International Conference on Mineral Exploration 355−374. Give URL

Ayer, J. A. and Trowell, N. F., 1998, Geological compilation of the Timmins area, Abitibi greenstone belt; Ontario Geological Survey, Preliminary Map P. 3379, scale 1:100000

Bartel, D. C., and Hohmann, G. W., 1985 Interpretation of Crone pulse electromagnetic data: Geophysics, **50**, 1488−1499.

Bartel, D. C., and Becker, A., 1988, Time-domain electromagnetic detection of a hidden target: Geophysics, **53**, 537−545.

Becker, A. , DeCarle, R. and Lazenby, P. G., 1984, Simplified prediction of the transient electromagnetic response: Geophysics, **49**, 913-917.

Chen, J. and Macnae, J. C., 1998, Automatic estimation of EM parameters in tau-domain: Exploration Geophysics, **29**, 170-174.

Davis, A. C., 2007, Quantitative characterization of airborne electromagnetic systmes: Ph.D. Thesis, RIMT University

Eaton, P. A., Anderson, R. G., Queen, S. V., Nilsson B. Y., Lauritsen, E., Barnett C. T., Olm M. and Mitchell, S., 2013, Helicopter time-domain electromagnetics- Newmont and the NEWTEM experience: Geophysics, **78**, W45−W56.

Grant, F. S., and West, G. F., 1965, Interpretation theory in applied geophysics: MacGraw Hill.

Kaufman, A. A., 1965, Theory of induction logging: Nauka, Siberian Division, Acad. Sci. U.S S.R.

Kaufman, A. A. 1978, Frequency and transient responses of electromagnetic field created by currents in confined conductors, Geophysics, **43**, 1002−1010.

Kuzmin P. V. and Morrison E. B., (2013) Bucking coil and b-field measurement system and apparatus for time domain electromagnetic measurements, US8400157B2.

Lane, R., Green, A., Golding, C., Owers, M., Pik, P., Plunkett, C., Sattel, D., Thorn, B., (2000) An example of 3D conductivity mapping using the TEMPEST airborne electromagnetic system: Exploration Geophysics, **31**, 162–172.

Macnae, J., 2012, Design and testing of ARMIT magnetic field sensors for EM systems: ASEG Extended Abstracts 1, 1-4

Macnae, J. C, Lamontagne, Y. and West, G. F. (1984). Noise processing techniques for time-domain EM systems, Geophysics, **49**, 934-948.

Martinez, J. M., Babic, S, and Akyel, C., 2014, On Evaluation of Inductance, dc- Resistance and Capacitance of Coaxial Inductors at Low Frequencies. IEEE Trans. Magn. **50**, 8401012-23

Nelson, P. H., and Morris, D. B., 1969, Theoretical response of a time-domain, airborne, electromagnetic system, Geophysics, **34**, 729-738.

Neri B, Pellegrini B., Saletti R. 1996, Ultra low-noise preamplifier for low-frequency noise measurements in electron devices, IEEE Trans. Instr. Meas., **40**, 2-6.

Ontario Geological Survey, 2003, Airborne magnetic and electromagnetic surveys, Reid-Mahaffy Airborne Geophysical Test Site Survey; Ontario Geological Survey, Geophysical Data Set−1045.

494 Ontario Geological Survey, 2004, Airborne magnetic and electromagnetic surveys
495 (2000−2002), Reid-Mahaffy Airborne Geophysical Test Site Survey; Ontario Geological
496 Survey, Geophysical Data Set−1111.

497 Palacky, G. J., and West, G. F., 1973, Quantitative interpretation of INPUT AEM
498 measurements, Geophysics, **38**, 1145-1158.

499 Press W. H, Teukolsky S. A. and Vetterling W.T. (2007) Numerical Recipes 3rd Edition: The
500 Art of Scientific Computing 3, Cambridge University Press New York, NY, USA.

501 Saini, H. S., Martinez J. M. Lopez L. 2014, The power converter stage of a powerful airborne
502 time domain electromagnetic system: 7th IET International Conference on Power Electronics,
503 Machines and Drives, Manchester (PEMD 2014). Can you give the URL?

504 Smith R. S and Annan, A. P., 2000, Using an induction coil sensor to indirectly measure the
505 B-field response in the bandwidth of the transient electromagnetic method: Geophysics, **65**,
506 1489-1494.

507 Smith, R. S. and Keating, P. B., 1996, The usefulness of multicomponent, time-domain
508 airborne electromagnetic measurements: Geophysics, **61**, 74-81.
509 https://doi.org/10.1190/1.1443958

510 Smith, R. S. and Lee, T. J., 2001, The impulse-response moments of a conductive sphere in an
511 uniform field, a versatile and efficient electromagnetic model: Exploration Geophysics, **32**,
512 113−118.

513 Sørensen K. I. and Auken, E. (2004) SkyTEM – a new high-resolution helicopter transient
514 electromagnetic system. Exploration Geophysics **35**, 194-202.

Stolz, E. M., and Macnae, J. C., 1998, Evaluating EM waveforms by singular-value decomposition of exponential basis functions: Geophysics, **63**, 64−74.

Xiao P., Shi Z., Wu X., and Fang G., 2017, Improved Bucking Coil Design in Helicopter Transient Electromagnetic System, PIER M, **60**, 131–139 can you give URL?

FIGURES

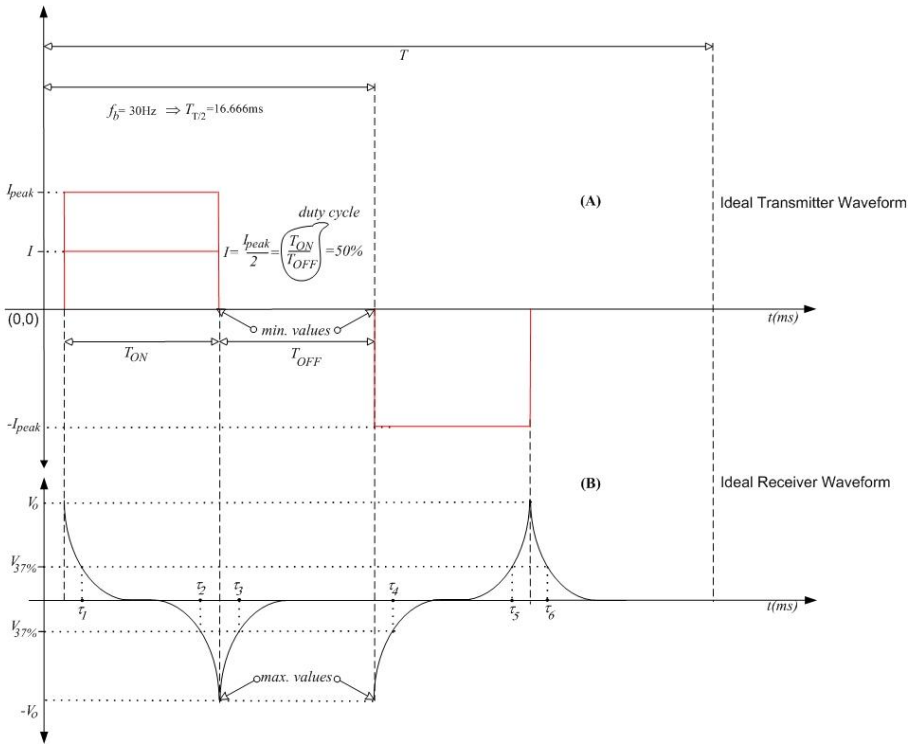

Figure 1. Full-cycle of ideal waveforms of an EM system (duty cycle = 50%)

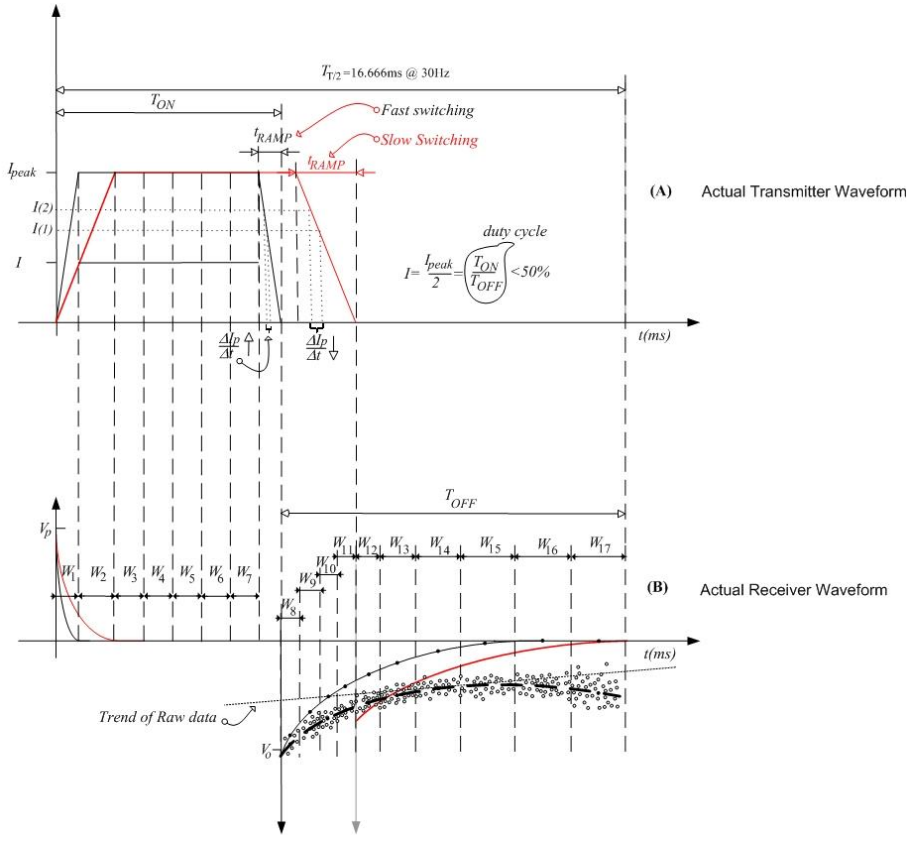

Figure 2. Half-cycle of actual waveforms of an AEM system driven by square pulse (duty cycle <50%)

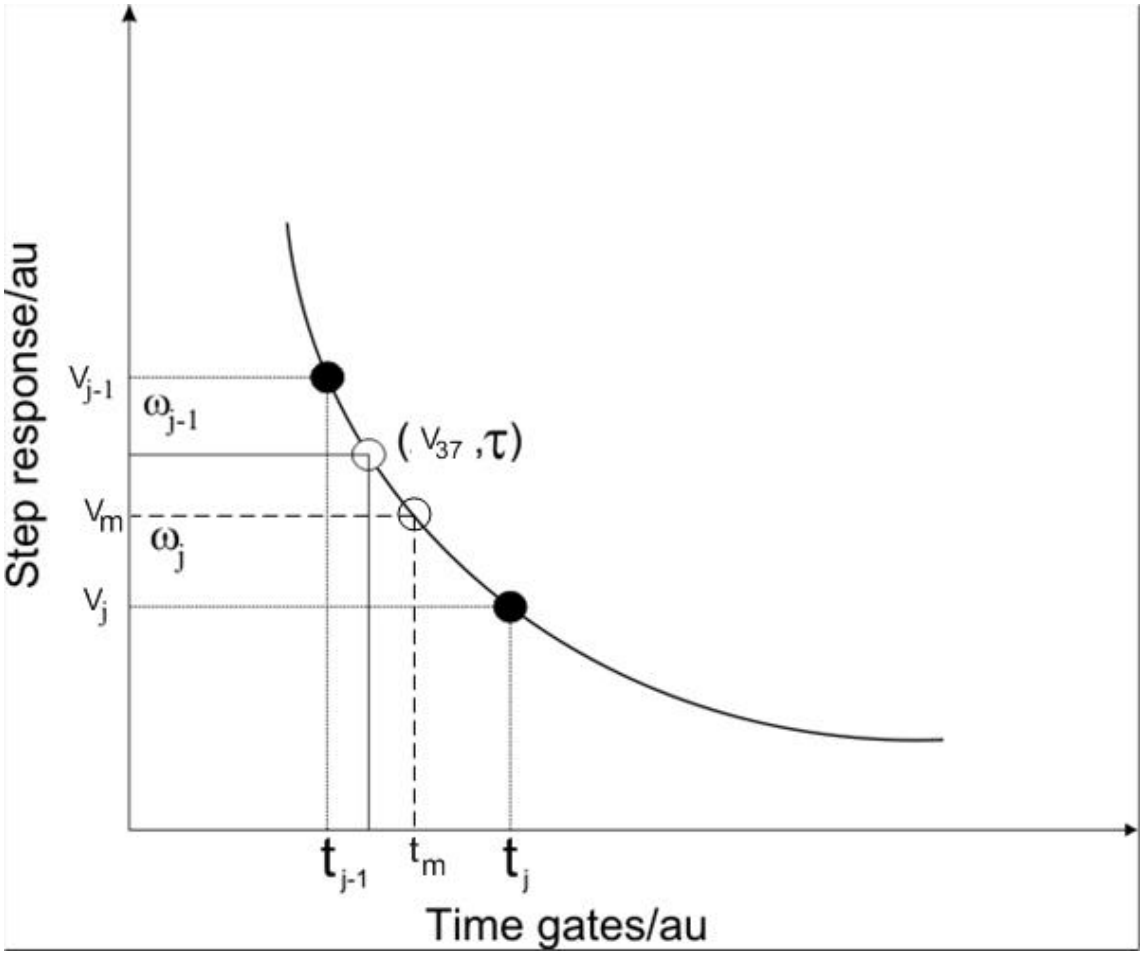

Figure 3 Schematics of V37-method to calculate τ from the time window table of AEM system.

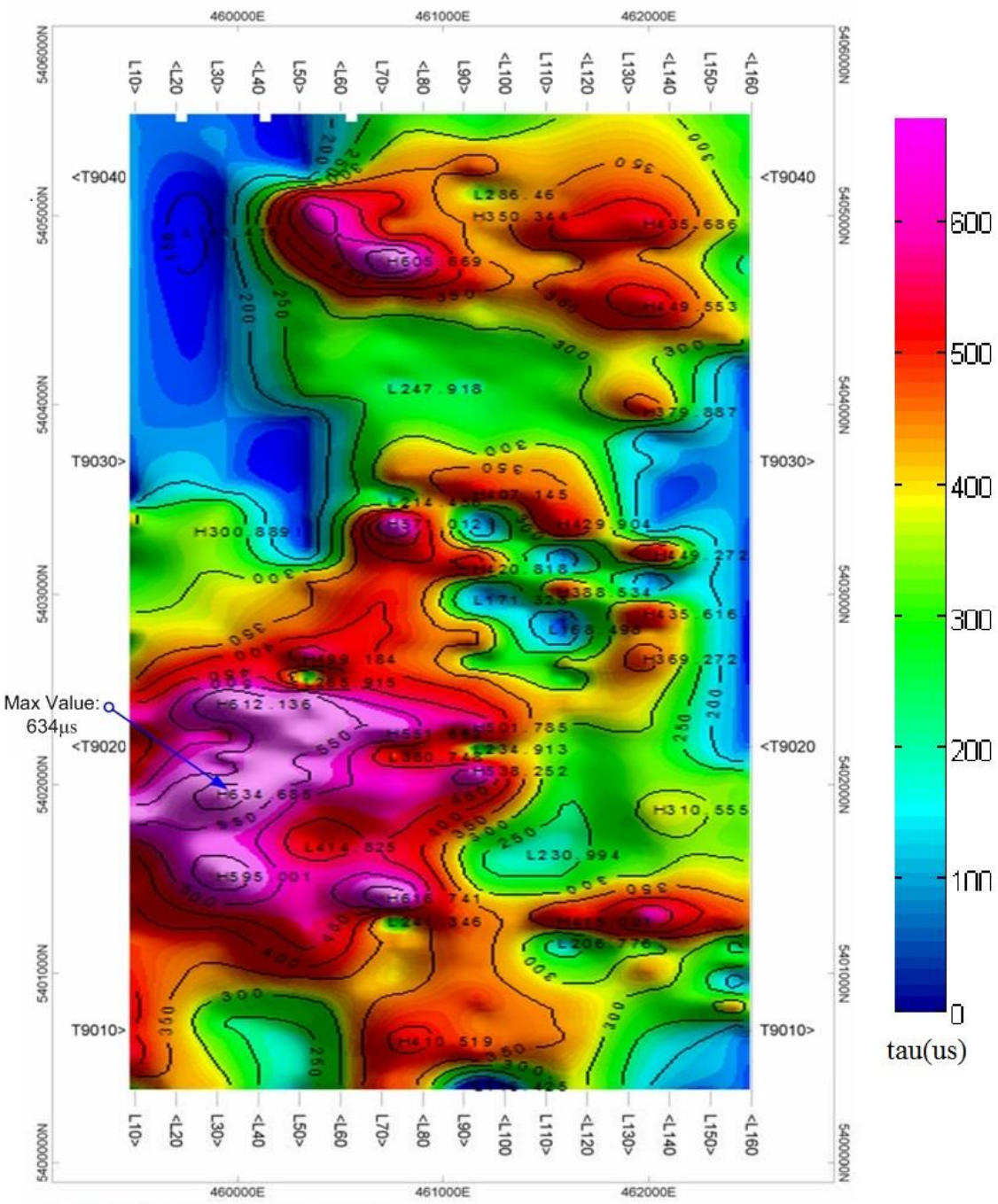

530

531 **Figure 4. The tau grid from W8 calculated using the standard method applied to fitting**

532 **of the Bz_channel of the darm1 EM database [OGS (2003)]**

533
534

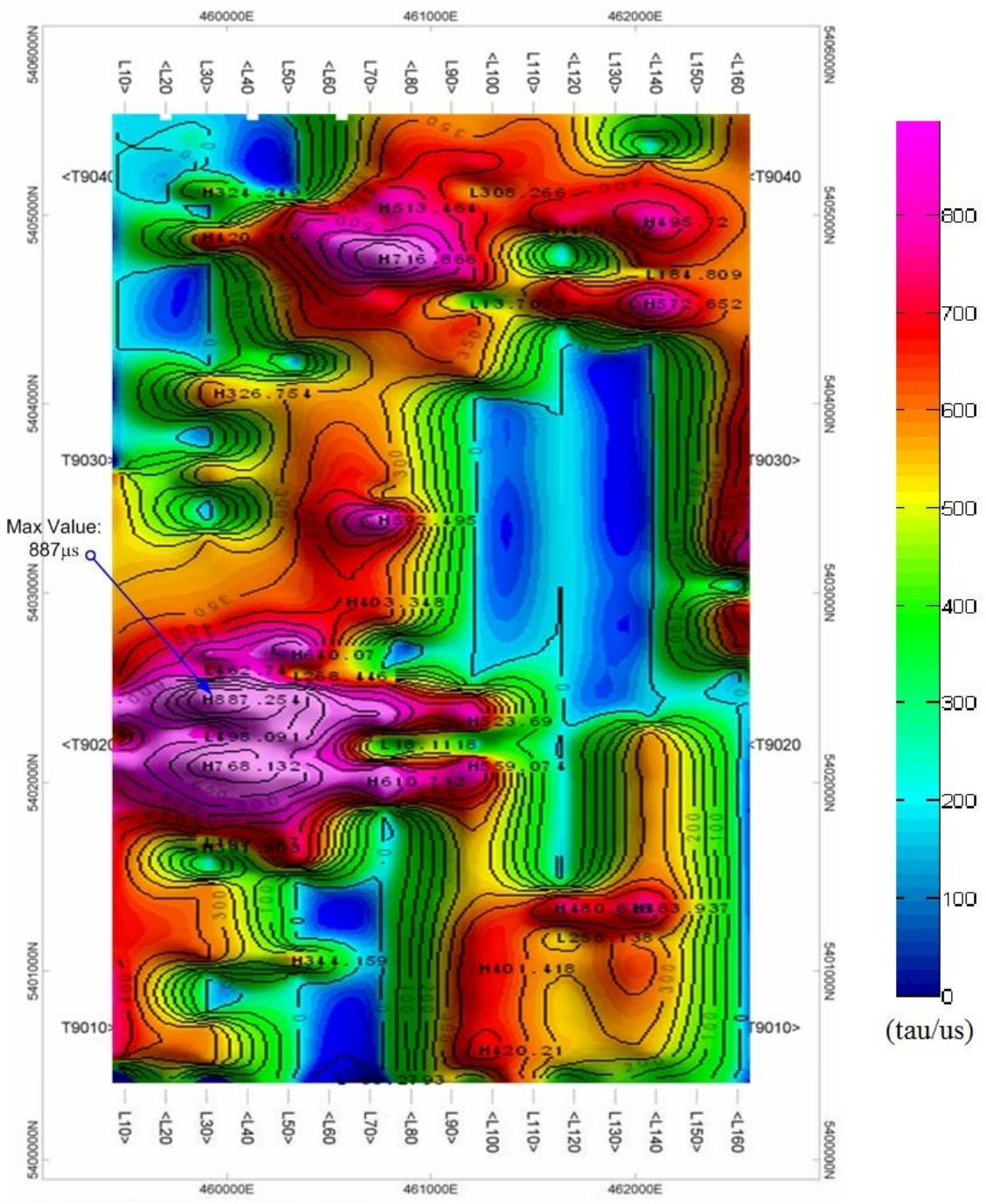

535

536 **Figure 5. The tau grid from W8 using V37-method (tol.=0%) from Bz channel of darm1**

537 **EM database [OGS (2003)]**

538

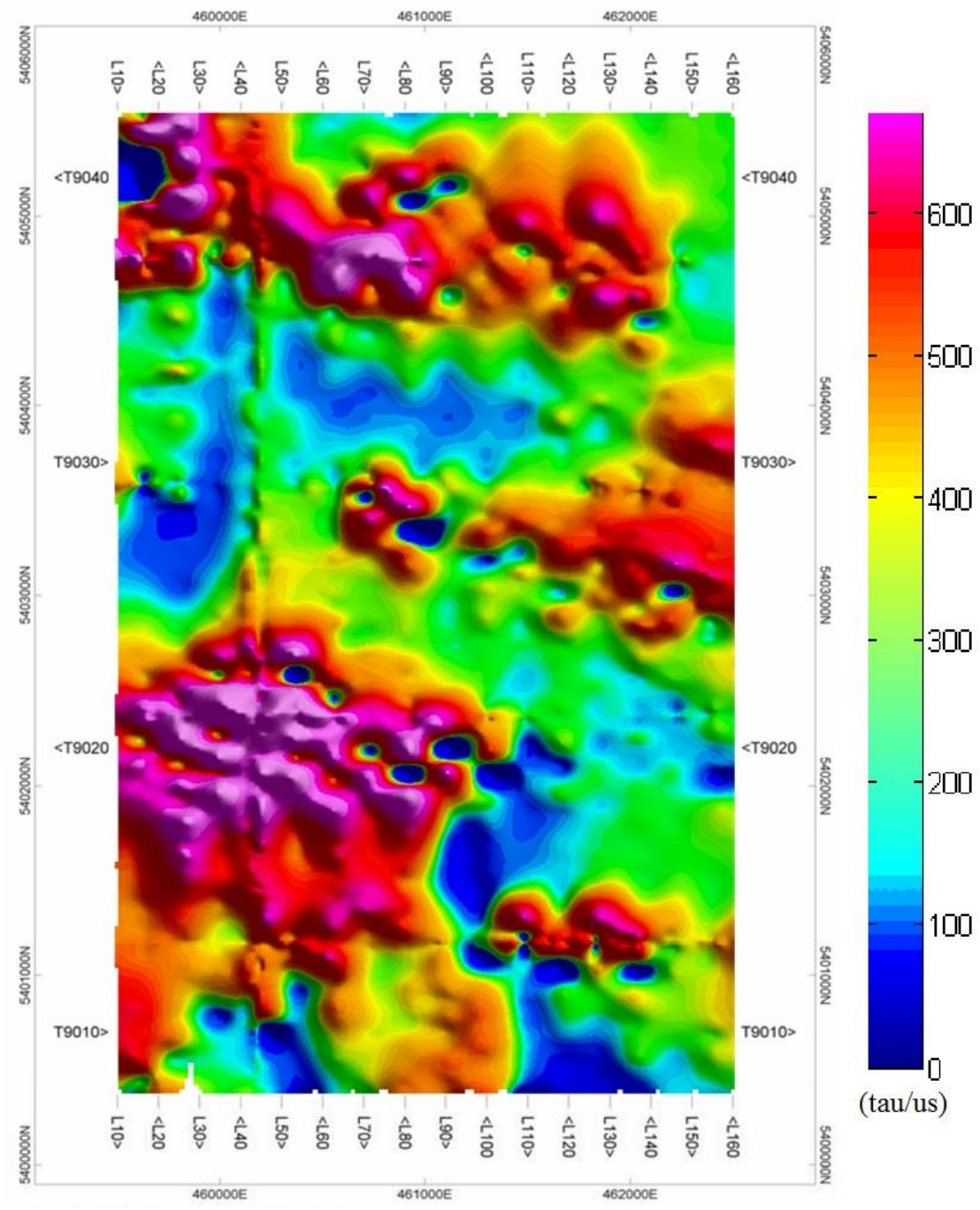
460000E
461000E
462000E
5406000N
5405000N
5404000N
5403000N
5402000N
5401000N
5400000N
L10>
<L20
L30>
<L40
L50>
<L60
L70>
<L80
L90>
<L100
L110>
<L120
L130>
<L140
L150>
<L160
<T9040
T9030>
<T9020
T9010>
600
500
400
300
200
100
0
(tau/us)

539

Figure 6. The tau grid from W8 using V37– method (tol.=5%) of the Bz_channel of darm2 EM database [OGS (2004)].

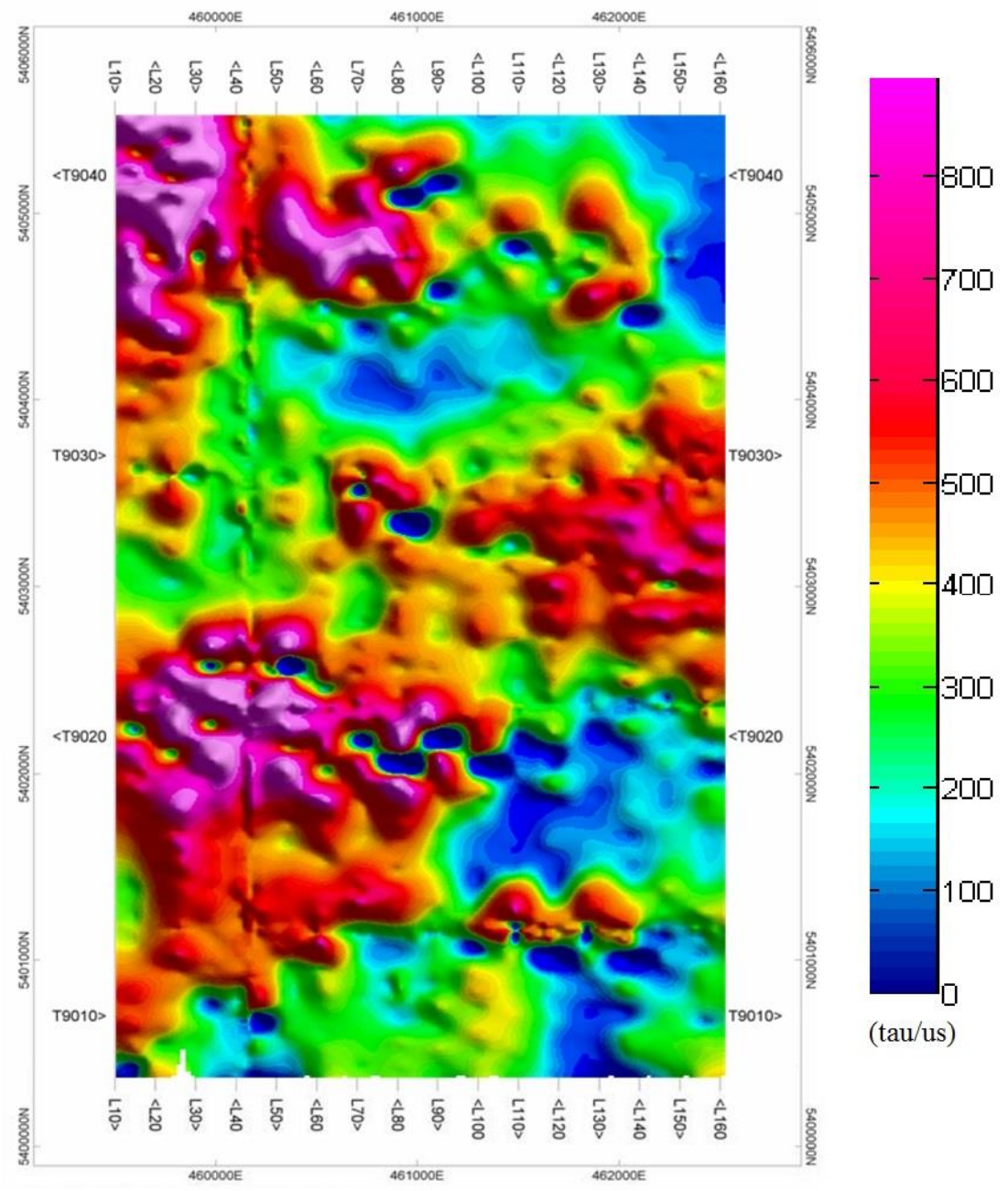

Figure 7. The tau grid from W9 using V37– method (tol.=5%) of the Bz_channel of darm2 EM database [OGS (2004)].

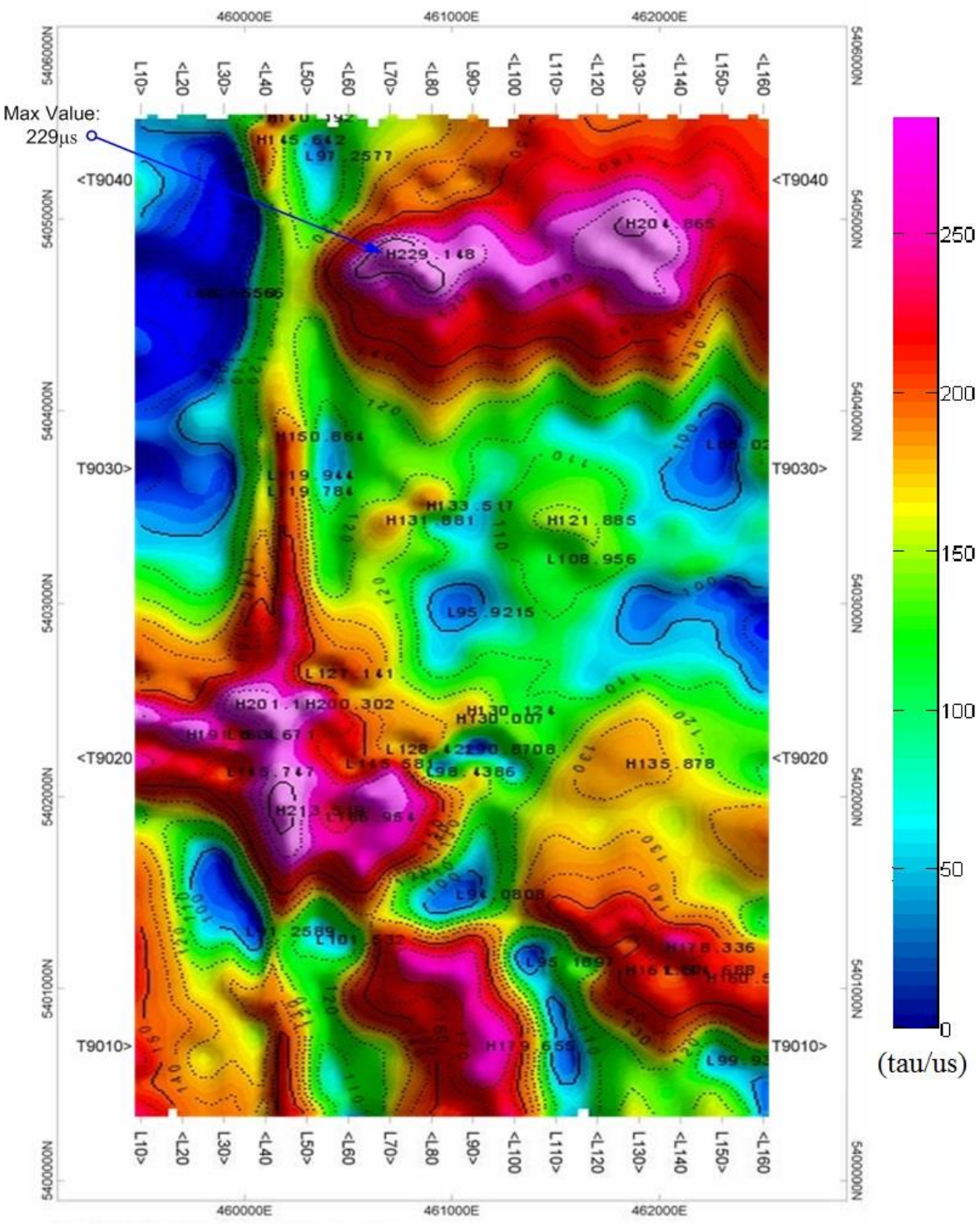
460000E
461000E
462000E
5406000N
5405000N
5404000N
5403000N
5402000N
5401000N
5400000N
L10>
<L20
L30>
<L40
L50>
<L60
L70>
<L80
L90>
<L100
L110>
<L120
L130>
<L140
L150>
<L160
Max Value:
229µs
<T9040
T9030>
<T9020
T9010>
H229.148
H204.865
H150.864
H133.517
H131.881
H121.885
L108.956
L95.9215
H135.878
H178.336
H179.655
250
200
150
100
50
0
(tau/us)

546

Figure 8. The tau grid from W8 using the standard method applied to fitting of the dBz/dt_channel of the darm2 EM database [OGS (2004)].

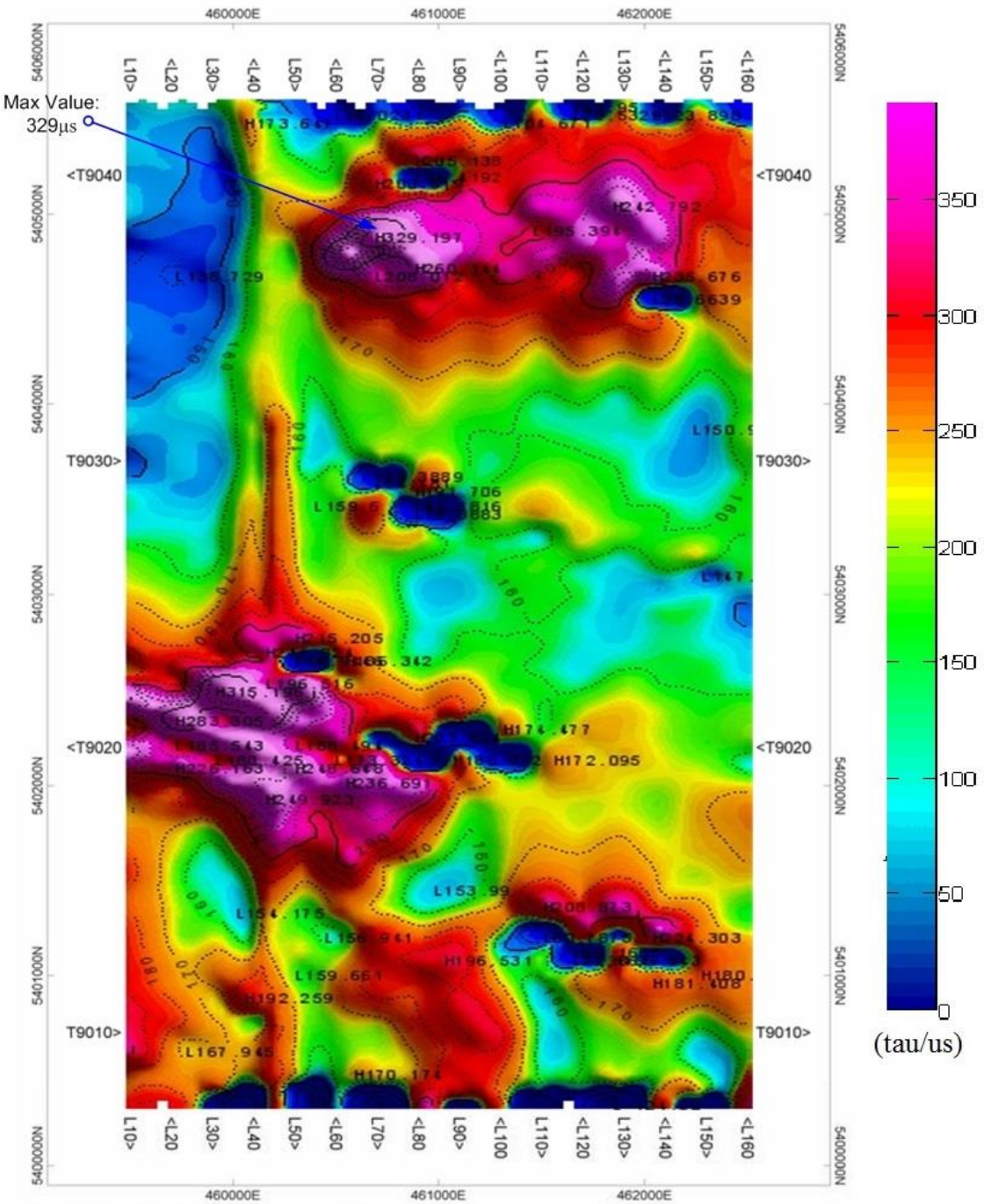

Figure 9. The tau grid from W8 using V37-method (tol.=5%)of dBz/dt_channel of darm2 EM database [OGS (2004)].

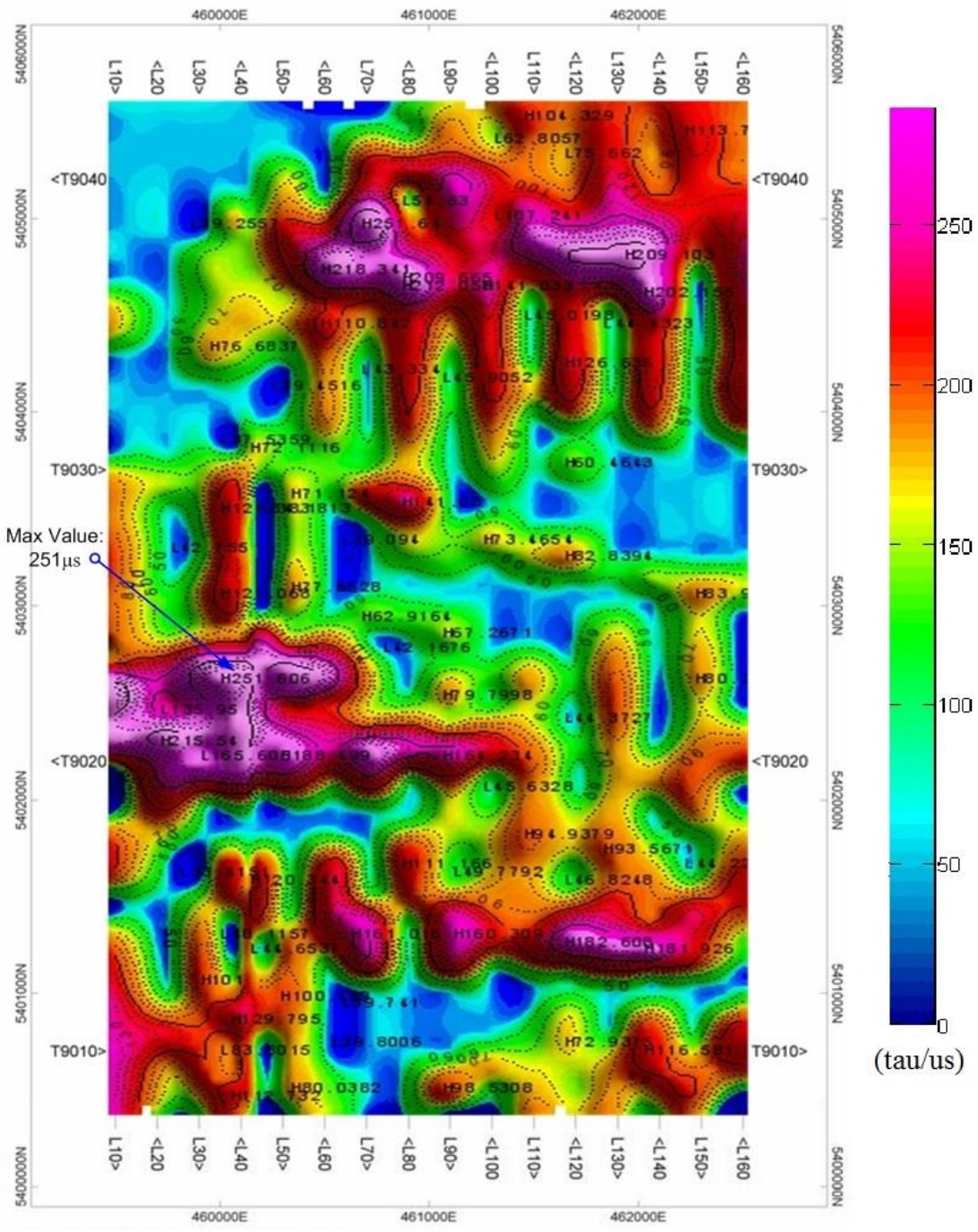

554

555 **Figure 10. The tau grid from W8 using the standard method of fitting the**

556 **dBx/dt_channel of the darm2 EM database [OGS (2004)].**

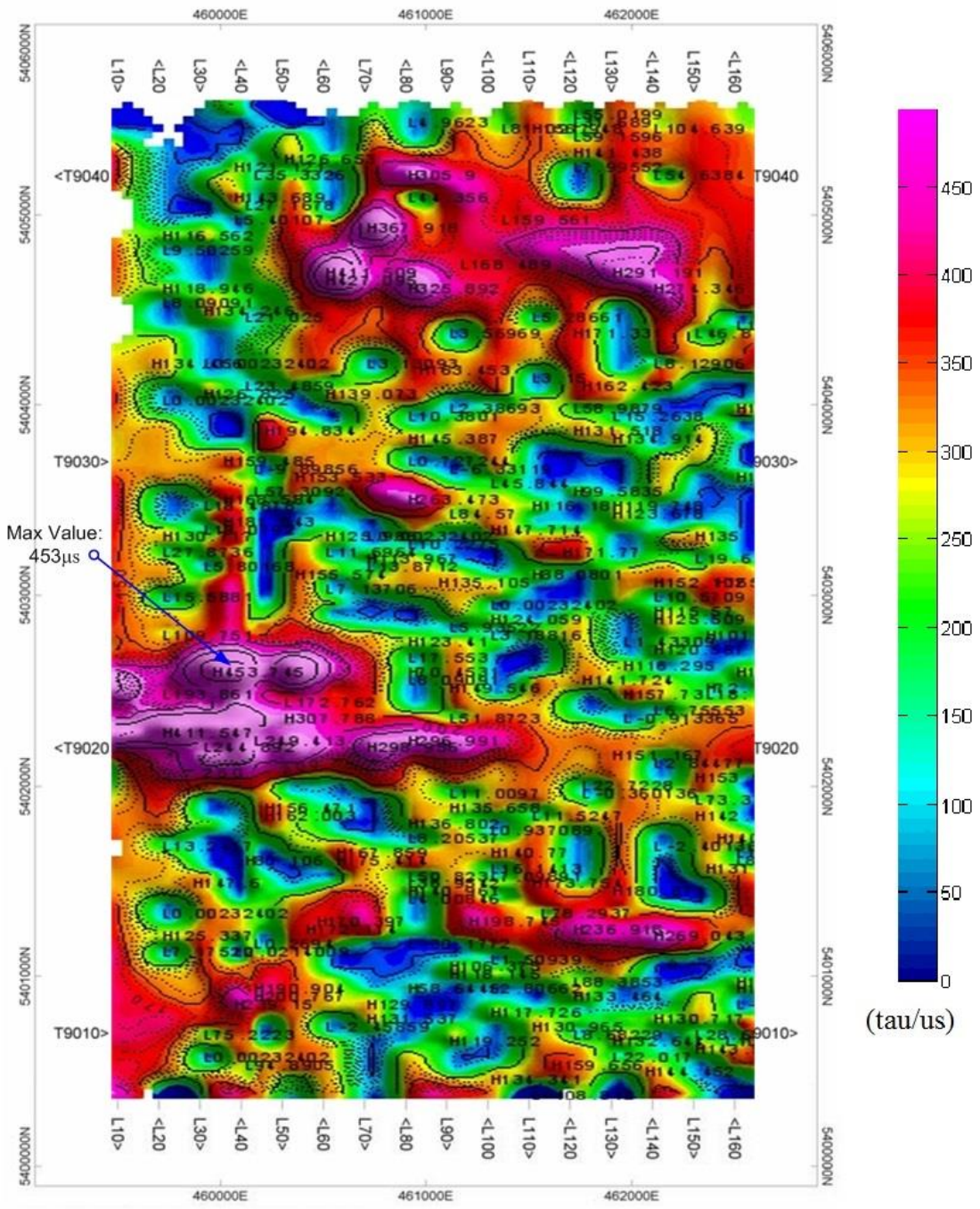

557

558 **Figure 11. The tau grid from W8 using V37-method (tol.=5%) of dBx/dt_channel of**

559 **darm2 EM database [OGS (2004)].**

560

561 **EQUATIONS**

562

563 $$\begin{matrix} V_z(t_j) \\ dV_z(t_j)/dt \end{matrix} = \begin{cases} V_0 e^{-t_j/\tau} \\ \frac{V_0}{\tau} e^{-t_j/\tau} \end{cases} \quad \begin{matrix} \textit{Step Response} \\ \textit{Impulse Response} \end{matrix} \qquad (1)$$

564 $$\tau = \omega_j t_j + \omega_{j-1} t_{j-1} \qquad (2)$$

565 $$\omega_{j-1} = \left(1 - \frac{V_{37} - V_{j-1}}{V_{j-1} - V_j}\right) \qquad (3)$$

566 $$\omega_j = \left(1 - \frac{V_j - V_{37}}{V_{j-1} - V_j}\right) \qquad (4)$$

567

568 **TABLE**

569

Survey	T (s)	f_b, (Hz)	v_h (m/s)	d (m)	N_t	N_s	Sample interval (μs)	m* Am^2
OGS2003	0.25	90	65	16	45	45	43.4	591 600
OGS2004	0.25	30	65	16	15	15	43.4	222 000
**actual moment of this survey*								

570

571 **Table. Survey parameters from MEGATEM II time-domain electromagnetic system**
572 **over**

573 **the Reid-Mahaffy test site**